https://doi.org/10.5194/egusphere-2022-673
Preprint. Discussion started: 23 August 2022

Semi-continuum modelling of unsaturated porous media flow to explain the Bauters' paradox

Jakub Kmec[1], Miloslav Šír[1], Tomáš Fürst[2], and Rostislav Vodák[2]

[1]Palacký University in Olomouc, Joint Laboratory of Optics of Palacky University and Institute of Physics of the Academy of Sciences of the Czech Republic, Faculty of Science, Olomouc, 771 46, Czech Republic
[2]Palacký University in Olomouc, Dpt. Mathematical Analysis and Applications of Mathematics, Faculty of Science, Olomouc, 771 46, Czech Republic

Correspondence: Jakub Kmec (jakub.kmec@upol.cz)

Abstract. In gravity-driven free infiltration of a wetting liquid into a homogeneous unsaturated porous medium, the flow pattern is known to depend significantly on the initial saturation. Point-source infiltration of a liquid into an initially dry porous medium produces a single finger with an oversaturated tip and an undersaturated tail. In an initially wet medium, a diffusion-like plume is produced with a monotonic saturation profile. We present a semi-continuum model based on a proper scaling of the retention curve which is discrete in space and continuous in time. We show that the semi-continuum model is able to describe this transition and to capture the experimentally observed dependence of the saturation overshoot and the finger velocity on the initial saturation.

1 Introduction

In the hydrological cycle, a total of $119000\ \mathrm{km}^3$ of precipitation per year falls on the land in the form of rain and snowfall. The volume of water in the soil in the form of moisture is $16000\ \mathrm{km}^3$. Worldwide, $148939200\ \mathrm{km}^2$ of land is covered by soil. From the land, $45000\ \mathrm{km}^3$ of water annually flows back to the ocean as surface runoff, and $2000\ \mathrm{km}^3$ flow as groundwater runoff. Thus, 0.04% of fresh water and 0.001% of total water in the hydrological cycle flows through the soil cover (Cahine, 1992; Kotwicki, 2009). How exactly precipitation water infiltrates into the soil remains a mystery, despite tremendous effort that has been devoted to infiltration research (Kutílek and Nielsen, 1994; Hunt et al., 2013). Even the simplest single-point source infiltration process is incredibly complex. This paper is dedicated to its elucidation.

Gravity driven free infiltration into an unsaturated porous medium usually follows preferred pathways through which most of the liquid flows leaving most of the medium dry (Glass et al., 1988). There are three types of preferential flow (Nimmo, 2021): Macropore flow, funnel flow, and finger flow. Macropore flow proceeds through individual large pores that are highly conductive. The funnel flow is the result of heterogeneity of soil or rock hydraulic properties. Both macropore flow and funnel flow are features of non-homogeneous porous media. However, preferential flow (also known as finger flow) also occurs in a homogeneous medium and is believed to be caused by the wetting front instability (Glass et al., 1989a; Bauters et al., 2000; Sililo and Tellam, 2005; Aminzadeh and DiCarlo, 2010; DiCarlo, 2013; Wei et al., 2014; Cremer et al., 2017; Pales et al., 2018). A finger consists of two parts: an oversaturated *finger tip* followed by a less saturated *finger tail*. It is widely accepted

https://doi.org/10.5194/egusphere-2022-673
Preprint. Discussion started: 23 August 2022

that this non-monotonicity of the saturation profile (i.e. saturation overshoot) is a necessary and sufficient condition of finger flow (DiCarlo, 2004; Rezanezhad et al., 2006).

It was experimentally observed that the magnitude of the saturation overshoot (i.e. the saturation difference between the finger tip and tail) depends on the infiltration rate (DiCarlo, 2004). For low influx, a stable wetting front forms without a saturation overshoot. For a larger flux, the saturation overshoot appears, and its magnitude increases with increasing flux up to a certain point beyond which the magnitude of the overshoot decreases again. For high flow rates, the saturation overshoot disappears completely. There is also a strong dependence of the flow regime on the initial saturation of the porous medium (Bauters et al., 2000). For an initially dry medium, finger flow accompanied by saturation overshoot is observed. However, at a sufficiently high initial saturation (close to the saturated moisture limit), fingers do not form and a stable front dominates with no saturation overshoot (see Fig. 3 in Bauters et al. (2000)). Moreover, a non-monotonic dependence of wetting front velocity and finger width on the initial saturation was reported. With increasing initial saturation, the fingers first become more narrow and faster, but further increase in initial saturation makes them slow down, become thicker and more irregular, and gradually disappear completely, giving way to diffusion-like plumes with no saturation overshoot. We call this complicated transition from finger-like regime to diffusion-like regime the *Bauters' paradox*, honoring the first author of the seminal article Bauters et al. (2000). Note that the preferential flow occurs also in highly saturated porous medium that is super-hydrophilic (Chen et al., 2022b). This complex behavior is not consistent with the standard theory which (1) does not allow for saturation overshoot behavior (Fürst et al., 2009), (2) predicts an increase in wetting front velocity with increasing initial saturation (Bear, 1972), and (3) does not allow for preferential flow in a homogeneous medium.

It is well known for a long time that the hydraulic and physical properties (e.g. porosity, pressure-saturation dependence, or permeability) of a porous medium are dependent on the sample volume (Larson and Morrow, 1981; Mishra and Sharma, 1988; Zhou and Stenby, 1993; Perfect et al., 2004; Ewing et al., 2010; Hunt et al., 2013; Ghanbarian et al., 2015, 2017, 2021). In classical continuum mechanics, this scaling problem is "defined away" by the concept of the Representative Elementary Volume (REV). REV is the smallest volume for which the key physical quantities (e.g. saturation and pressure) can still be considered smooth. However, if a sample is used smaller than the REV, the effect of the scaling is significant and the continuum assumption is violated (Kouznetsova et al., 2001; White et al., 2006; Al-Raoush and Papadopoulos, 2010; Al-Raoush, 2012). Note that REV is usually very small in structural mechanics and fluid mechanics. However, in the case of common porous media, the REV is much larger. This makes traditional continuum mechanics-based modelling of porous media flow inappropriate because we are primarily interested in the description of flow phenomena below the REV scale.

The standard model for unsaturated porous media flow is the Richards' Equation (RE) (Richards, 1931). RE is a combination of a mass balance equation and the Darcy-Buckingham law (Bear, 1972). It was shown by means of a mathematical proof that in the case of a constant influx into an initially dry homogeneous porous medium, RE is incompatible with saturation overshoot (Fürst et al., 2009). Thus, RE is not able to capture finger flow. There have been many attempts to compensate for this inadequacy; in principle, these attempts can be divided into continuum models (Hassanizadeh et al., 2002; Eliassi and Glass, 2002; Schneider et al., 2017; Brindt and Wallach, 2020; Beljadid et al., 2020; Cueto-Felgueroso et al., 2020; Ommi et al., 2022a, b), and pore-scale (discrete) models (Lenormand et al., 1983, 1988; Wilkinson, 1986; Blunt and Scher, 1995; Primkulov

https://doi.org/10.5194/egusphere-2022-673
Preprint. Discussion started: 23 August 2022

et al., 2018, 2019; Wei et al., 2022). Another approach is to combine the advantages of continuous and discrete modelling (Glass and Yarrington, 1989, 2003; Liu et al., 2005; Liu, 2017). Liu et al. (2005) and Liu (2017) developed an active region model in which fractal flow patterns are incorporated into the continuum approach. Glass and Yarrington (1989, 2003) proposed a unique Macro Modified Invasion Percolation model (MMIP), which is – in a single framework – able to capture finger flow, buoyancy-driven migration of gases through porous media, and rough surface flow. However, saturation is not treated as a continuous quantity in the MMIP model, thus the model cannot reproduce the saturation overshoot or its dependence on initial saturation or influx rate. For a detailed review of the different types of modelling, see e.g. Rooij (2000); DiCarlo (2010); Xiong (2014); Chen et al. (2022a).

Another attempt is reported in Kmec et al. (2019, 2021), who advocate for the so-called semi-continuum approach. In this approach, the porous medium is divided into a grid of blocks which are not considered infinitesimal – each block retains the nature of a porous medium and it is characterized by its pressure–saturation relation, hydraulic conductivity, and porosity. Saturation is considered continuous in time but constant throughout each block (i.e. piecewise constant in space). Flow between neighboring blocks proceeds according to the Darcy-Buckingham law. The key feature of the semi-continuum approach is to account for the block size. This is done by an appropriate scaling of the retention curve with the block size (Vodák et al., 2022). As the block size decreases, the retention curve becomes more flat (i.e. its derivative decreases) while keeping the hysteresis effect constant. See Vodák et al. (2022) for more details and a physical justification.

The semi-continuum model was shown to reproduce well all experimentally observed features of unsaturated porous medium flow in a long vertical tube (Kmec et al., 2019). A two dimensional version of the model was shown to correctly capture the transition between finger flow and diffusion-like flow with increasing initial saturation (Kmec et al., 2021) for uniform infiltration imposed on the entire top boundary. Vodák et al. (2022) examined the limit of the semi-continuum model as the block sizes go to zero. They report a limit version of the model in the form of a partial differential equation with a Prandtl-type hysteresis operator (Visintin, 1993) under the derivative. The limit equation switches between parabolic and hyperbolic type and it seems to form a new type of mathematical models of Nature.

In this paper, we demonstrate that the semi-continuum model is able to fully reproduce the Bauters' paradox – the transition from finger-like flow in initially dry medium to diffusion-like flow in initially wet medium for a point source infiltration. We show that the non-monotonic relation between initial saturation and flow velocity, and initial saturation and saturation overshoot magnitude is captured correctly by the semi-continuum model.

1.1 Bauters' paradox

The authors of Bauters et al. (2000) used a Hele-Shaw cell ($50 \times 30 \times 0.94$ cm) filled with homogeneous $20/30$ quartz sand with particle size between 0.60 mm and 0.85 mm. Water was injected at a rate of 2 cm^3 min^{-1} through a hypodermic needle located at the top of the chamber near the sand surface. The initial saturation was gradually increased from zero to the full field capacity. The results of the experiments can be summarized as follows:

https://doi.org/10.5194/egusphere-2022-673
Preprint. Discussion started: 23 August 2022

- *Wetting front dependence on the initial saturation.* As the initial saturation increases, the flow regime changes from an unstable finger-like to a stable diffusion-like flow. Three flow regimes can be distinguished: unstable, intermediate, and stable. During unstable flow, the finger width remains almost constant. This is consistent with theoretical analysis (Raats, 1973) and experimental observations (Selker et al., 1992; Rezanezhad et al., 2006). In the intermediate regime, the fingers gradually give way to a stable infiltration front. This type of flow transition has not yet been sufficiently investigated, either theoretically or experimentally. In the diffusion-like regime, the saturation and pressure profiles are monotonic with no overshoot behavior. Moreover, the wetting front is much wider than the finger.
- *The width and velocity of the fingers.* With increasing initial saturation, the fingers first become faster and narrower, then they get slower and wider.
- *Pressure and saturation overshoot magnitude.* The magnitude of the saturation overshoot decreases with increasing initial saturation of the medium. Moreover, a hyperbolic relation between initial saturation and saturation overshoot magnitude is observed. The same holds for the pressure overshoot magnitude.

Although the experiments of Bauters et al. (2000) are well known in the soil science community (currently almost 90 citations in the Scopus database), there is no unified explanation for the observed paradox. Moreover, almost none of the citing authors comment on this interesting phenomenon. To our best knowledge, there are only three attempts to model or explain Bauters' paradox. Chapwanya and Stockie (2010) used a dynamic capillary pressure term to model the effect of initial saturation. However, a small artificial perturbation in the influx had to be used to initiate the finger flow, and the influx was imposed over the entire top boundary instead of a point. The finger velocity was independent of the initial saturation of the medium. Moreover, the authors did not focus on the non-monotonic dependence of finger width on initial saturation.

Another attempt was undertaken by Joekar-Niasar and Hassanizadeh (2012) and Masoodi and Pillai (2012). The authors hypothesized that the non-monotonic velocity of the front is due to a trade-off between conductivity and capillary pressure. With increasing initial saturation, the conductivity increases because there is more trapped air in the medium. Beyond a critical value of initial saturation, the trapping does not change significantly, but the matric potential decreases. As a result, the wetting front slows down. This means that the intrinsic permeability of the medium is not a constant but a function of saturation.

Finally, Kmec et al. (2021) used a semi-continuum approach to investigate the effect of the initial saturation on the wetting flow formation. Similar to Chapwanya and Stockie (2010), the influx was imposed on the entire top boundary. The nonlinear dependence of the finger width was reproduced (see Fig. 6 in Kmec et al. (2021)). The finger velocity dependence on the initial saturation was not studied due to different choice of the top boundary condition than in Bauters et al. (2000).

This article presents simulations of the point source infiltration used in Bauters et al. (2000) by means of the semi-continuum model. We show that all the experimentally observed features of the Bauters' paradox are reproduced well.

https://doi.org/10.5194/egusphere-2022-673
Preprint. Discussion started: 23 August 2022

2 Methods

2.1 Semi-continuum model

Let us recall the 2D semi-continuum model that was introduced by Kmec et al. (2021). Here, we use the same model with an appropriate scaling of the retention curve with the block size (Vodák et al., 2022). The porous medium is represented as a rectangular grid of $N \times M$ square blocks of uniform size $\Delta x \times \Delta x$. Each block is denoted by its row and column indices $[i,j]$. Saturation $S_t(i,j)$ and pressure $P_t(i,j)$ of the wetting phase (liquid) at time t are assumed constant within each block (i,j), and the pressure of the non-wetting phase (gas) is assumed to be zero everywhere. Each block retains the nature of a porous medium and it is characterized by a hysteretic pressure–saturation relation (main wetting branch $p^w(S)$, main draining branch $p^d(S)$), non-hysteretic hydraulic conductivity (intrinsic permeability κ, relative permeability $k(S)$), and porosity θ. The invading wetting liquid is characterized by its density ρ and dynamic viscosity μ. Acceleration due to gravity is denoted by g. The semi-continuum model tracks the following three key quantities: The saturation $S_t(i,j)$ $[-]$ of the wetting phase in each block at time t, the pressure $P_t(i,j)$ [Pa] of the wetting phase in each block at time t, and the fluxes $q_t[(i_1,j_1) \rightarrow (i_2,j_2)]$ $[\mathrm{ms}^{-1}]$ of the wetting phase between neighboring blocks (i_1,j_1) and (i_2,j_2) at time t.

At each instant, the saturation in each block is updated according to the discretized mass balance law in the following way:

$$\frac{\theta}{\Delta t}\left[S_{t+\Delta t}(i,j) - S_t(i,j)\right] = \tag{1}$$
$$= \frac{1}{\Delta x}\left[q_t[(i-1,j) \rightarrow (i,j)] - q_t[(i,j) \rightarrow (i+1,j)] + q_t[(i,j-1) \rightarrow (i,j)] - q_t[(i,j) \rightarrow (i,j+1)]\right),$$

where θ $[-]$ denotes the porosity of the material, Δt is a time step, and Δx is the block size. A backward scheme can be also used (Kmec et al., 2021) but it slows the numerical algorithm unnecessarily.

The next step is to update the capillary pressure in each block according to the capillary pressure operator $P(S)$. The capillary pressure operator consists of the main wetting and draining branches defined by van Genuchten equation (5). To complete the capillary pressure operator, a hysteresis model is included (Parker and Lenhard, 1987). We use a similar approach to the play-type hysteresis used, e.g., in Rätz and Schweizer (2013); Schweizer (2017). All scanning curves are straight lines with a very large gradient K_{PS}. Once a block (in the wetting mode between the two main branches) reaches the main wetting branch along a scanning curve, it clings to it and continues along it. A similar procedure applies for the block in the draining mode.

Finally, the flux between neighboring blocks is updated according to the Darcy-Buckingham law (Bear, 1972):

$$q = \frac{\kappa}{\mu} k(S)\left(\rho g - \nabla P(S)\right), \tag{2}$$

where κ $[\mathrm{m}^2]$ denotes the intrinsic permeability, ρ $[\mathrm{kgm}^{-3}]$ the fluid density, g $[\mathrm{ms}^{-2}]$ acceleration due to gravity, and μ [Pas] the dynamic viscosity of fluid, and $P(S)$ is the capillary pressure operator. The relative permeability function $k(S)$ is modelled by the form derived in Mualem (1976); Mualem and Dagan (1978); Van Genuchten (1980):

$$k(S) = S^{\lambda}\left[1 - \left(1 - S^{\frac{1}{m}}\right)^{m}\right]^2, \tag{3}$$

https://doi.org/10.5194/egusphere-2022-673
Preprint. Discussion started: 23 August 2022

where λ $[-]$ is a free parameter. Let us denote by $\gamma(S) = \kappa k(S)$ the effective permeability of the porous medium.

We use the following discrete implementation of the Darcy-Buckingham law (2):

$$q_t[(i_1,j_1) \to (i_2,j_2)] = \begin{cases} \frac{1}{\mu}\sqrt{\gamma(S_t(i_1,j_1)\gamma(S_t(i_2,j_2)}\left(\rho g - \frac{P_t(i_2,j_2)-P_t(i_1,j_1)}{\Delta x}\right) & \text{for } j_1 = j_2,\ i_2 = i_1+1 \\ \frac{1}{\mu}\sqrt{\gamma(S_t(i_1,j_1)\gamma(S_t(i_2,j_2)}\left(0 - \frac{P_t(i_2,j_2)-P_t(i_1,j_1)}{\Delta x}\right) & \text{for } i_1 = i_2,\ j_2 = j_1+1 \\ 0 & \text{otherwise} \end{cases} \tag{4}$$

Thus, for the hydraulic conductivity between blocks, we use the geometric mean of the conductivity values in the respective blocks. This choice of averaging has the desirable property of being small if the permeability of one of the blocks is small. The force of gravity is included only for the vertical fluxes $j_1 = j_2$. After setting the fluxes between neighboring blocks, the time is updated to $t + \Delta t$ and we proceed back to Eq. (1).

2.2 Scaling of the retention curve

A crucial idea behind the semi-continuum model is the appropriate scaling of the main branches of the retention curve which was first introduced by Vodák et al. (2022). The scaling of the retention curve is based on the fact that the shape of the retention curve depends on the size (especially the height) of the sample on which the measurement is made (Larson and Morrow, 1981; Hunt et al., 2013; Silva et al., 2018).

The simple scaling mechanism introduced in Vodák et al. (2022) is used here in which the main branches of the retention curve take the form of the standard van Genuchten model (Van Genuchten, 1980). For more details about the proposed scaling of the retention curve and its sample size dependency, see the discussion in Vodák et al. (2022).

For the reference block size Δx_0, the retention curve is modelled by the formula

$$p_0^w(S) = -\frac{1}{\alpha_w}\left(S^{\frac{-1}{m_w}} - 1\right)^{\frac{1}{n_w}}, \qquad p_0^d(S) = -\frac{1}{\alpha_d}\left(S^{\frac{-1}{m_d}} - 1\right)^{\frac{1}{n_d}}, \tag{5}$$

where S denotes saturation, p_0^w is the capillary pressure on the wetting branch, p_0^d is the capillary pressure on the draining branch, α_w, n_w, and $m_w = 1 - \frac{1}{n_w}$ are parameters of the main wetting branch, and α_d, n_d, and $m_d = 1 - \frac{1}{n_d}$ are parameters of the main draining branch.

The idea of the retention curve scaling is the following. For block size $\Delta x < \Delta x_0$, the retention curve becomes more flat but the distance between the main wetting and draining branches remains the same. Thus for the main wetting branch

$$p^w(S, \Delta x) = \frac{\Delta x}{\Delta x_0} p_0^w(S) + c^w \tag{6}$$

with c^w such that $p^w(0.5, \Delta x) = p_0^w(0.5)$, i.e.

$$c^w(\Delta x) = p_0^w(0.5)\left(1 - \frac{\Delta x}{\Delta x_0}\right). \tag{7}$$

Clearly, for $\Delta x = \Delta x_0$, relation (6) reduces to equation (5) while for $\Delta x \to 0$, we obtain $p^w(S, \Delta x) \to p_0^w(0.5)$. For the main draining branch $p^d(S, \Delta x)$ the scaling is analogous to Eq. (6) and (7).

https://doi.org/10.5194/egusphere-2022-673
Preprint. Discussion started: 23 August 2022

The scaling of the retention curve for $20/30$ sand is shown in Fig. 1 for the reference block size $\Delta x_0 = \frac{10}{12}\ \mathrm{cm} \approx 0.83\ \mathrm{cm}$. Determining the dimension of Δx_0 is not trivial. It is explained in Sect. 3 how this dimension can be determined using the results of Bauters et al. (2000).

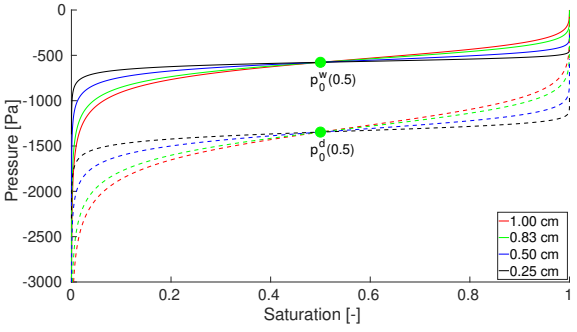

Figure 1. The scaling of the retention curve for $20/30$ sand. The solid lines denote the main wetting branches and the dashed lines denote the main draining branches for the respective value of Δx. The green curve represents the reference sample for $\Delta x_0 = \frac{10}{12}\ \mathrm{cm} \approx 0.83\ \mathrm{cm}$. As $\Delta x \to 0$, the retention curve becomes more flat but the distance between the main wetting and draining branches remains the same. The main wetting and draining branches "rotate" around fixed values $p_0^w(0.5)$ and $p_0^d(0.5)$, respectively.

3 Results

We want to completely reproduce the experiments reported in Bauters et al. (2000). The authors report that water was injected at a rate of $2\ \mathrm{cm}^3\ \mathrm{min}^{-1}$ through a hypodermic needle located near the sand surface. Thus, a point source infiltration is modeled such that a constant flux is prescribed across one centimeter of the top edge (in the middle). Zero discharge at the bottom boundary is prescribed, for simplicity. This choice of the bottom boundary condition does not affect the studied phenomena. All parameters used for the simulations are given in Table 1. The parameter $\lambda = 0.8$, which is consistent with experimental measurements (Schaap and Leij, 2000).

3.1 Adjustment of reference block size for 20/30 sand

First of all, the reference block size Δx_0 is unknown. This is a parameter of the semi-continuum model that has to be set. The parameter Δx_0 was calibrated by simulating the experiments of Bauters et al. (2000). In the simulation, we use the parameters for 20/30 sand adopted from Schroth et al. (1996) and DiCarlo (2004) (see Table 1). We ran several simulations of the semi-continuum model with Δx_0 equal to $\frac{10}{12}\ \mathrm{cm}$, $1.00\ \mathrm{cm}$ and $\frac{12}{10}\ \mathrm{cm}$. The moisture profile was calculated for three different initial saturation: a dry (0.001), a medium dry (0.01) and a wet (0.05) porous medium. The parameters used for simulations are given in Table 1, except for the block size $\Delta x = 0.50\ \mathrm{cm}$ and $A = 17\ \mathrm{cm}$ (horizontal width of the chamber), which were changed in order for the simulations not to be extremely time consuming. The moisture profiles for all values of Δx_0 are depicted in Fig. 2.

https://doi.org/10.5194/egusphere-2022-673
Preprint. Discussion started: 23 August 2022

Parameter	Symbol	Value
Horizontal width of the chamber	A	31 cm
Vertical length of the chamber	B	50 cm
Reference block size	Δx_0	0.83 cm
Block size	Δx	0.25 cm
Porosity	θ	0.35
Density of water	ρ	1000 kgm^{-3}
Dynamic viscosity of water	μ	9×10^{-4} Pas
Intrinsic permeability	κ	2.294×10^{-10} m^2
Relative permeability exponent	λ	0.8
Acceleration due to gravity	g	9.81 ms^{-2}
Wetting curve parameter	α_w	0.177 cm^{-1}
Wetting curve parameter	n_w	6.23
Draining curve parameter	α_d	0.0744 cm^{-1}
Draining curve parameter	n_d	8.47
Slope of scanning curves	K_{PS}	10^5 Pa
Boundary flux	q_B	8×10^{-5} ms^{-1}

Table 1. Parameters used to reproduce the experiments of Bauters et al. (2000). Parameters for 20/30 sand were adopted from Schroth et al. (1996) and DiCarlo (2004).

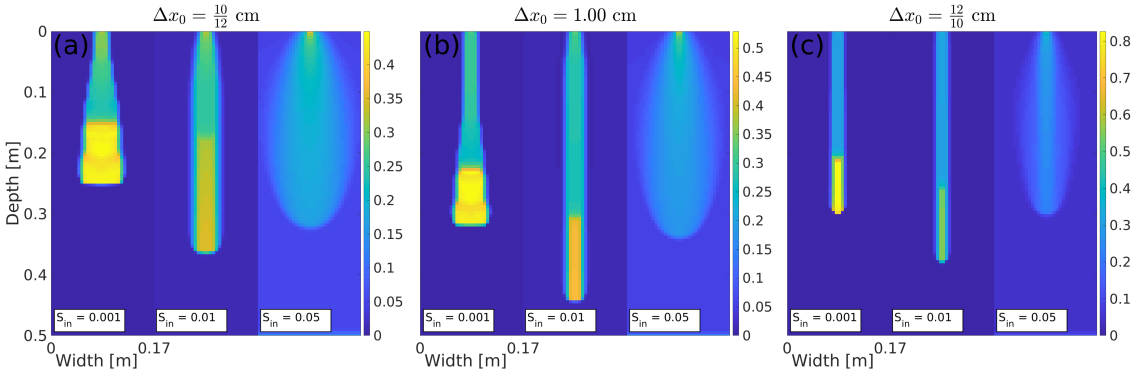

Figure 2. Snapshots of the saturation field for various Δx_0 for initially dry ($S_{in} = 0.001$), a medium dry ($S_{in} = 0.01$) and a wet ($S_{in} = 0.05$) porous material. The moisture profiles for **(a)** $\Delta x_0 = \frac{10}{12}$ cm, **(b)** $\Delta x_0 = 1.00$ cm and **(c)** $\Delta x_0 = \frac{12}{10}$ cm are shown at 30, 30 and 20 minutes, respectively. Saturation values are colour-coded according to the colour bar on the right.

We want to choose the parameter Δx_0 for which the non-monotonic behavior of the moisture profiles widths occurs. Table 2 shows the width of the moisture profiles. The width of the moisture profile is calculated in the following way: First, we calculate

https://doi.org/10.5194/egusphere-2022-673
Preprint. Discussion started: 23 August 2022

the width of each row, which equals $n_{row} \times \Delta x$, where n_{row} is a number of blocks in the row for which the saturation exceeds 0.07 during the simulation and Δx is the size of the block. The width of the moisture profile is then calculated as the average width of all rows with non-zero width. It is clear that the most pronounced non-monotonic behavior of the moisture profiles widths is given for $\Delta x_0 = \frac{10}{12} \approx 0.83$ cm (Fig. 2a), and is therefore the most appropriate.

reference block size Δx_0	moisture profile width for:		
	$S_{in} = 0.001$	$S_{in} = 0.01$	$S_{in} = 0.05$
$\frac{10}{12}$ cm	5.3137 cm	4.6986 cm	8.1000 cm
1.00 cm	4.0156 cm	3.8202 cm	7.8500 cm
$\frac{12}{10}$ cm	2.6333 cm	2.8421 cm	4.6200 cm

Table 2. The width of the moisture profiles for different values of Δx_0.

Note that the width of the finger is not constant for initially dry porous medium, although it is experimentally observed (Bauters et al., 2000). This artificial behavior is due to the unrealistic homogeneity of porous medium used for the simulation. Although, in reality, the porous medium is homogeneous, this does not mean that all the characteristics are identical in each block of the simulation. If a small distribution of the intrinsic permeability is included, the finger width will be constant. This is demonstrated in the next section.

3.2 Wetting front dependence on initial saturation

Let us now demonstrate the ability of the semi-continuum model to capture the Bauters' paradox. As mentioned above, even in homogeneous porous medium, all characteristics are not identical in each block. Thus, the spatially correlated distribution of the intrinsic permeability is introduced. Such distribution was also used e.g in Kmec et al. (2021). The distribution satisfies $\kappa_{max}/\kappa_{min} \approx 4$ and the mean of the intrinsic permeability approximately equals κ. The distribution of the values of intrinsic permeability is shown in Fig. 3. The distribution of the intrinsic permeability is not the cause of the Bauters' paradox. However, with such a distribution, more physical-looking fingers evolve. For a simulation of the Bauters' paradox without the intrinsic permeability distribution, see Fig. 4.3 in Kmec (2021).

Figure 4 shows a snapshot of the saturation field at 25 minutes for seven different values of the initial saturation. It can be seen that as the initial saturation increases, the finger first gets faster and narrower. Then the finger slows down and widens and finally gives way to a diffusion-like plume. The transition between unstable and stable flow is also in agreement with the experimental observation: The non-monotonic behavior of the finger width and velocity is captured correctly as well as the shape of the wetting front. Moreover, a stable wetting front appears for initial saturation higher than 0.03, which is also consistent with experiments. Note that the authors of Bauters et al. (2000) only recorded the wetting front patterns 15 cm from the top. Therefore, we are not able to compare the wetting fronts at the upper part of the chamber.

https://doi.org/10.5194/egusphere-2022-673
Preprint. Discussion started: 23 August 2022

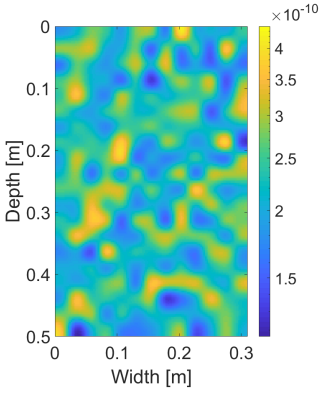

Figure 3. The distribution of the intrinsic permeability, which satisfies $\kappa_{max}/\kappa_{min} \approx 4$. Intrinsic permeability values are colour-coded according to the colour bar on the right.

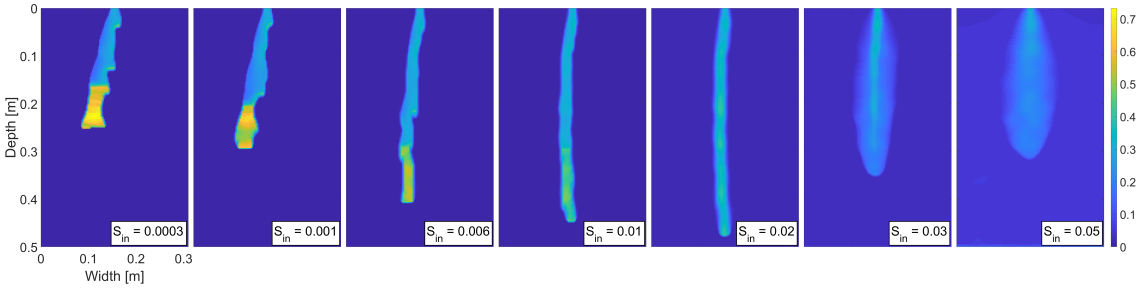

Figure 4. Snapshot of the saturation field at 25 minutes for seven different values of the initial saturation. Saturation values are colour-coded according to the colour bar on the right. Initial saturation of the medium increases from left to right.

One may wonder if this complex behavior depends on the choice of the intrinsic permeability distribution. We generated seven different distributions (see Fig. A1) and the same simulations as above were performed. Snapshots of the saturation field 25 minutes from the beginning of the infiltration for seven different values of the initial saturation are shown in Fig. A2 - A8. The figures show that the character of the flow remains the same for all types of distributions. Thus, the distribution of the intrinsic permeability does not affect the transition from the finger flow to the diffusion-like flow.

3.3 Width and velocity of the fingers

Figure 5a shows the width of the fingers (moisture profiles) 25 minutes from the beginning of infiltration for the simulation shown in Fig. 4 (wetting profiles for $S_{in} = 0.0005,\ 0.002,\ 0.04$ are not included in Fig. 4). The width of each moisture profile is calculated in the same way as was used in Table 2. We can clearly see that the finger width first slightly decreases and then increases. The narrowest finger is produced for $S_{in} = 0.01$ (2.70 cm) which is consistent with experiments (see Fig. 5 in Bauters et al. (2000)). Let us note that the finger width for $S_{in} = 0.0003$ (3.74 cm) is slightly smaller than for $S_{in} = 0.0005$

https://doi.org/10.5194/egusphere-2022-673
Preprint. Discussion started: 23 August 2022

(3.82 cm). However, this is due to the distribution of the intrinsic permeability. Indeed, the finger width for all simulations given by eight different distributions of the intrinsic permeability (see Fig. 3 and Fig. A1) is depicted in Fig. 5b. We observe that – on average – the finger width for the lowest initial saturation used in the simulation is higher than for $S_{in} = 0.0005$.

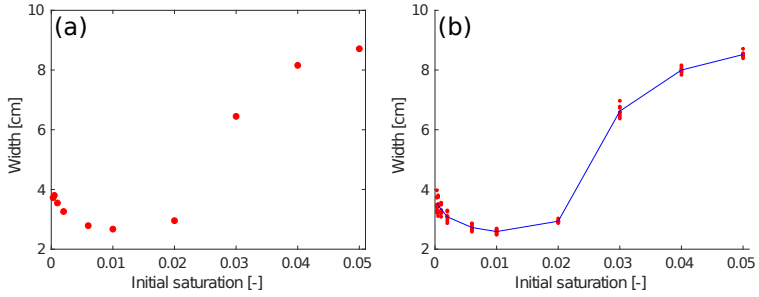

Figure 5. The width of the finger (or wetting front) at $t = 25$ minutes is plotted against the initial saturation. **(a)** For the distribution of the intrinsic permeability given by Fig. 3. **(b)** For all simulations given by eight different distributions of the intrinsic permeability (see Fig. 3 and Fig. A1). The blue line connects the averages.

For finger velocity, we proceed similarly, i.e., we find the bottom-most block of the finger whose saturation exceeds 0.07. The depth of the bottom-most block defines the current length of the finger. Finger velocity is computed as the rate of change of the finger length in time. The finger (or wetting front) velocity at $t = 25$ minutes for the simulation given by Fig. 4 is summarized in Fig. 6a. The advance of the wetting front was slower for the diffusion-like behavior compared to finger flow (but higher than for $S_{in} = 0.002$). This is rather counter-intuitive, since the classical Richards' Equation predicts an increase in velocity with increasing initial saturation. The highest finger velocity is observed for $S_{in} = 0.02$, and it is approximately five times lower than the highest finger velocity experimentally observed in Bauters et al. (2000) (for $S_{in} = 0.01$). This is consistent because we used four times lower influx in our simulations compared to the experiments. We observed that the character of the dependence remains the same for different distributions of the intrinsic permeability (see Fig. 6b).

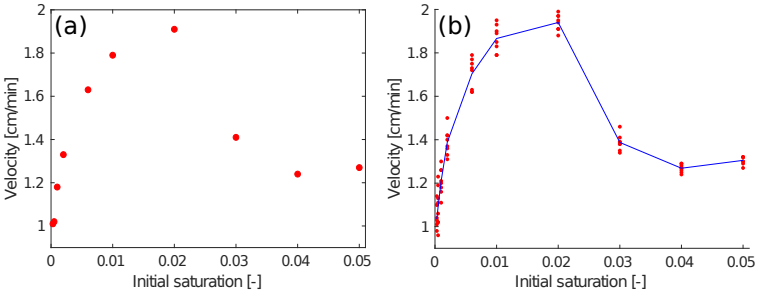

Figure 6. The velocity of the wetting front at $t = 25$ minutes is plotted against the initial saturation. **(a)** For the distribution of the intrinsic permeability given by Fig. 3. **(b)** For all simulations given by eight different distributions of the intrinsic permeability (see Fig. 3 and Fig. A1). The blue line connects the averages.

https://doi.org/10.5194/egusphere-2022-673
Preprint. Discussion started: 23 August 2022

3.4 Water content at and behind the wetting front

Let us now examine the change in saturation at and behind the wetting front (a finger tip). The difference between the saturation of the tip and the tail is called the saturation overshoot magnitude. To quantify the saturation overshoot magnitude, the saturation is averaged for each row, which gives the saturation profiles in 1D. Averaging is applied only to those blocks whose saturation exceeds 0.07. Saturation overshoot magnitude is then given as an average saturation at the finger tip minus an average saturation at the finger tail. In the case of diffusion-like flow with no overshoot, we average the bottom 20 centimeters of the saturation profile and subtract the average of the rest of the profile.

The dependence of saturation overshoot magnitude on initial saturation at $t = 25$ minutes is shown in Fig. 7. We see that there is a hyperbolic decay relationship between the initial saturation and the saturation overshoot magnitude ($R^2 = 0.990$). This is consistent with the experimental observation (Bauters et al., 2000). There is still a minor saturation overshoot for $S_{in} = 0.02$. This is again consistent with the experiments, where the authors observed a saturation overshoot for $S_{in} = 0.02$, but no overshoot for $S_{in} = 0.03$.

Let us note that the distribution of the intrinsic permeability causes higher variability in the saturation profiles. Without this distribution, the accuracy of the fit is better. This was shown in the 1D semi-continuum model, where the hyperbolic fit was obtained with $R^2 = 0.995$ (see Fig. 3.6. in Kmec (2021)).

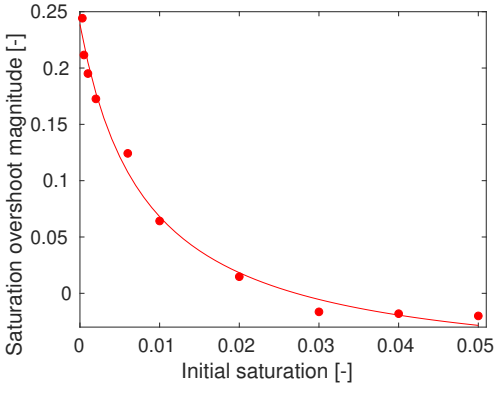

Figure 7. Dependence of the saturation overshoot magnitude on initial saturation at 25 minutes. Saturation overshoot magnitude is computed even for diffusion-like profiles (see the text for the methodology). A hyperbolic relation $f(x) = \frac{ax+b}{cx+d}$ fitted to the simulated data has a R^2 value of 0.990.

4 Discussion

To our best knowledge, the presented semi-continuum model is the first model which is able to fully capture the Bauters' paradox. This is achieved without introducing any new parameters, or material functions. The semi-continuum model is based on well established physics only – mass balance equation, the Darcy-Buckingham law, and a proper scaling of the retention

https://doi.org/10.5194/egusphere-2022-673
Preprint. Discussion started: 23 August 2022

curve with the volume of the block. The model may help to explain the precise mechanism of the transition between the finger-like and diffusion-like regimes.

A distribution of intrinsic permeability was used in the model. This was motivated by the following observation: As the blocks get smaller and smaller, the variability of their material characteristics necessarily increases. The characteristic of a block is given by an average over the pores of the block. As the block size decreases, so does the number of pores over which the average is taken. Thus, the variability of the characteristics increases. It is possible to introduce a distribution of other parameters such as porosity and the parameters of the retention curve (White et al., 2006; Ghanbarian et al., 2021). However, to keep the model as simple as possible, this has not been implemented here. It should be stressed that the Bauters' paradox appears even if the intrinsic permeability is kept homogeneous.

DiCarlo states the following four criteria to evaluate a model for unsaturated porous media flow (DiCarlo, 2013). Paraphrasing his words, the model should

1. have a minimum of adjustable parameters, and the parameters should be meaningful,
2. reduce to the RE in non-overshoot and static profiles,
3. produce a good match of the observed 1D profiles, not just the magnitude of the overshoot,
4. be able to produce predictions of the 2D and 3D preferential flow in terms of finger widths and finger spacing.

Since the RE can simulate only a diffusion-like regime, we understand (2) in the way that the model should be able to reproduce also diffusion-like regime, not only the fingering regime.

The semi-continuum model formulation uses only the physics of the Richards' Equation (porosity, permeability, the pressure-saturation relation, mass conservation, and the Darcy-Buckingham Law). The block size used in the simulation is not a free parameter – it is tied to the retention curve by the scaling relation and the reference block size Δx_0. The value of Δx_0 is not arbitrary, it is connected to the REV. Thus, item 1 of DiCarlo's list is satisfied. In view of Fig. 4, 5, 6, 7 and the results in Kmec et al. (2019, 2021), we claim items 2–4 are also satisfied.

However, there are two exceptions: For 2D preferential flow, the dependence of finger width and finger spacing on the influx is still missing. Here, we mention, for example, the experiments of Yao and Hendrickx (1996) for low infiltration rates and Glass et al. (1989b) for higher infiltration rates. We will discuss this complex dependency in a forthcoming paper. Moreover, the semi-continuum model has not yet been extended to 3D.

It should be noted that the semi-continuum model is not a numerical scheme to solve Richards' Equation. The difference between the semi-continuum model and a numerical scheme for the Richards' Equation is twofold: (1) An appropriate scaling of the retention curve with the block size is included for the semi-continuum model, and (2) geometric mean of the relative permeability is used for computing the flux between neighboring blocks. If (1) and (2) were not utilized in the semi-continuum model, diffusion-like flow patterns would always be produced with a monotonic saturation profile. This behavior is demonstrated for the initially almost dry medium in Fig. 8. The used distribution of the intrinsic permeability is shown in Fig. 3. A typical finger with saturation overshoot is produced for the semi-continuum model (Fig. 8a), while without (1) and (2), a monotonic diffusion-like profile is formed (Fig. 8b). In Vodák et al. (2022) we have demonstrated that the overshoot behavior

https://doi.org/10.5194/egusphere-2022-673
Preprint. Discussion started: 23 August 2022

is not lost in the limit $dx \to 0$. Thus, the semi-continuum model does not converge to the Richards' Equation, even if the block size goes to zero. It converges to a new type of hysteretic partial differential equation that – to our knowledge – has not been studied so far. We invite the porous media community to study the semi-continuum model and its limit because so far, it has been proven to capture well all of the complex and counter-intuitive features of unsaturated homogeneous porous media flow that have been observed and reported in the literature.

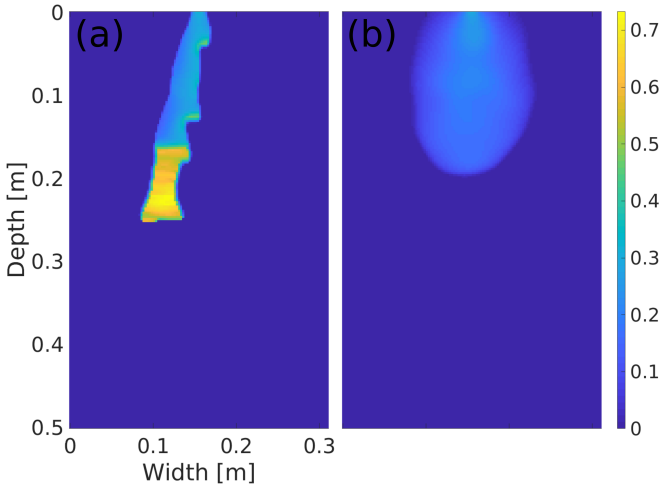

Figure 8. A comparison between the semi-continuum model and the Richards' Equation. Richards' Equation does not utilize the scaling of the retention curve and geometric mean of the relative permeability. Snapshot of the saturation field for **(a)** the semi-continuum model and **(b)** the Richards' Equation (right) at $t = 25$ minutes for $S_{in} = 0.0003$. Saturation values are colour-coded according to the colour bar on the right.

5 Conclusions

It is known from infiltration experiments that unsaturated porous media flow patterns depend on the initial saturation of the medium in a complex way. Going from initially dry to initially wet medium, the flow pattern changes from finger-like regime with a pronounced saturation overshoot to a diffusion-like regime with no overshoot. During the transition, several finger characteristics (velocity, overshoot magnitude, finger width) change in a non-monotonic way. This complex behavior is called the Bauters' paradox and the standard continuum mechanics-based theory has been unable to reproduce it.

Here, we introduced a semi-continuum model (discrete in space, and continuous in time) which is able to correctly reproduce all the observed features of the Bauters' paradox. The semi-continuum model implements a physically relevant scaling of the retention curve – the slope of the retention curve decreases with decreasing block size. This model correctly reproduces the flow patterns both for initially dry, and initially wet porous medium.

https://doi.org/10.5194/egusphere-2022-673
Preprint. Discussion started: 23 August 2022

Code and data availability. The software code that produced the simulations is written in MatLab and can be downloaded from Kmec (2022). Simulation data that are needed to create the plots included in the manuscript can be downloaded from Kmec et al. (2022). Please do not hesitate to contact us if you encounter any problems when downloading the software code and simulation data.

https://doi.org/10.5194/egusphere-2022-673
Preprint. Discussion started: 23 August 2022

Appendix A

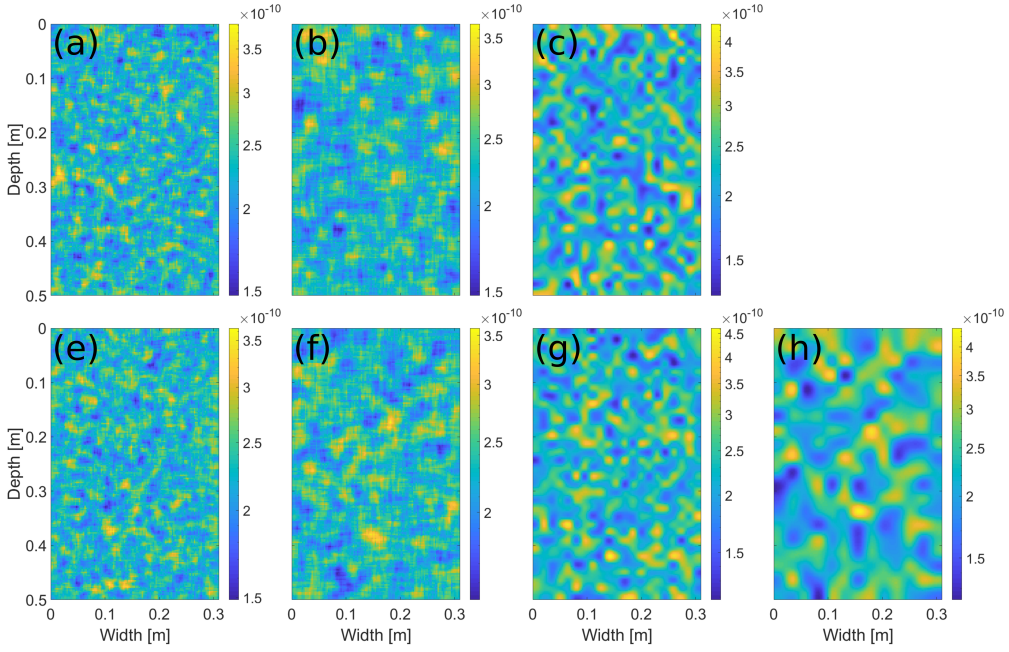

Figure A1. The distribution of the intrinsic permeability. The distributions satisfy: **(a)** $\kappa_{max}/\kappa_{min} \approx 2.60$, **(b)** $\kappa_{max}/\kappa_{min} \approx 2.50$, **(c)** $\kappa_{max}/\kappa_{min} \approx 3.40$, **(e)** $\kappa_{max}/\kappa_{min} \approx 2.45$, **(f)** $\kappa_{max}/\kappa_{min} \approx 2.35$, **(g)** $\kappa_{max}/\kappa_{min} \approx 3.90$, **(h)** $\kappa_{max}/\kappa_{min} \approx 3.50$. Intrinsic permeability values are colour-coded according to the colour bar on the right.

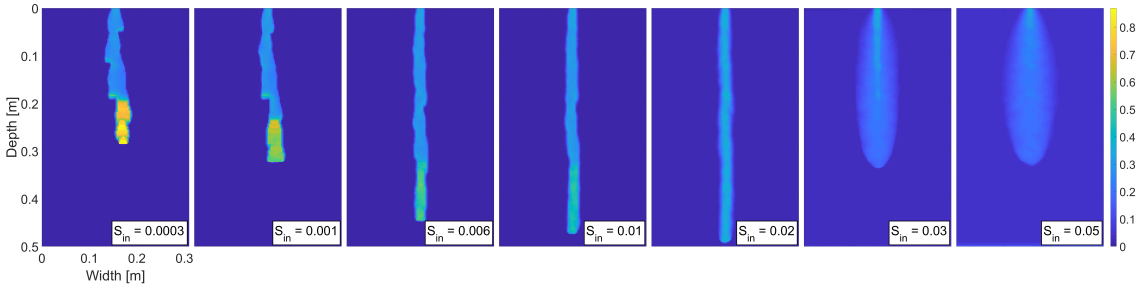

Figure A2. Snapshot of the saturation field at 25 minutes for seven different values of the initial saturation for the distribution which satisfies $\kappa_{max}/\kappa_{min} \approx$ 2.60 (the distribution in Fig. A1a). Saturation values are colour-coded according to the colour bar on the right.

https://doi.org/10.5194/egusphere-2022-673
Preprint. Discussion started: 23 August 2022

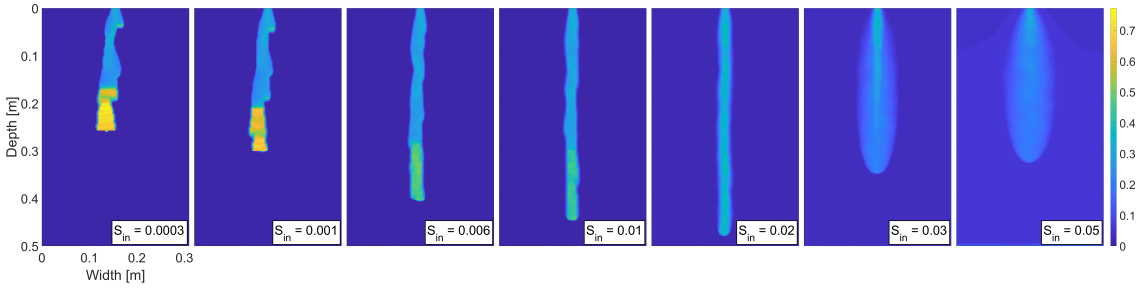

Figure A3. Snapshot of the saturation field at 25 minutes for seven different values of the initial saturation for the distribution which satisfies $\kappa_{max}/\kappa_{min} \approx 2.50$ (the distribution in Fig. A1b). Saturation values are colour-coded according to the colour bar on the right.

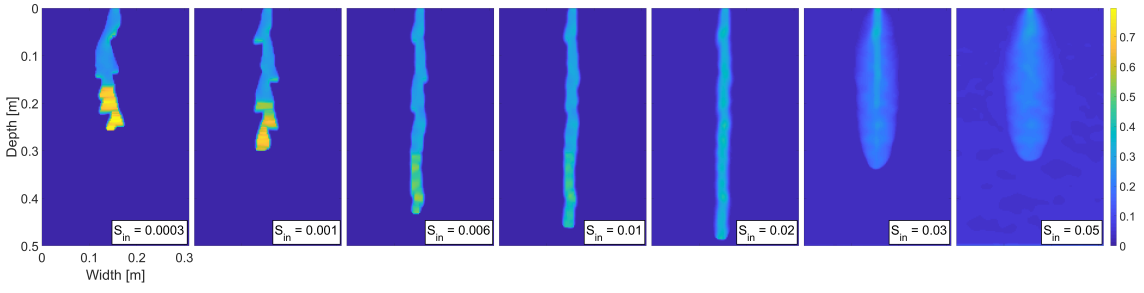

Figure A4. Snapshot of the saturation field at 25 minutes for seven different values of the initial saturation for the distribution which satisfies $\kappa_{max}/\kappa_{min} \approx 3.40$ (the distribution in Fig. A1c). Saturation values are colour-coded according to the colour bar on the right.

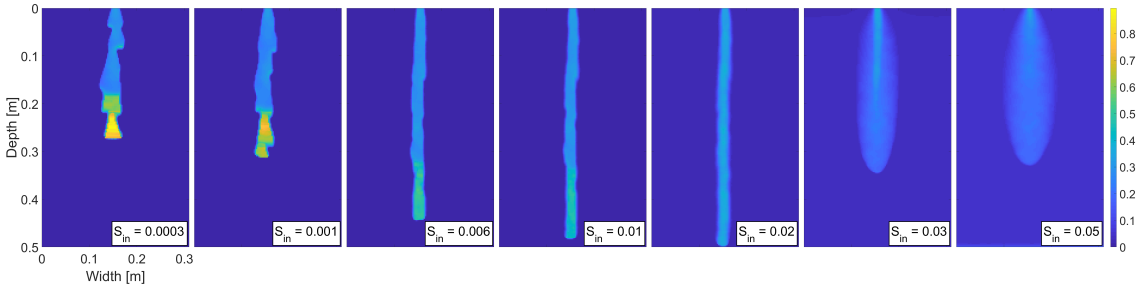

Figure A5. Snapshot of the saturation field at 25 minutes for seven different values of the initial saturation for the distribution which satisfies $\kappa_{max}/\kappa_{min} \approx 2.45$ (the distribution in Fig. A1e). Saturation values are colour-coded according to the colour bar on the right.

https://doi.org/10.5194/egusphere-2022-673
Preprint. Discussion started: 23 August 2022

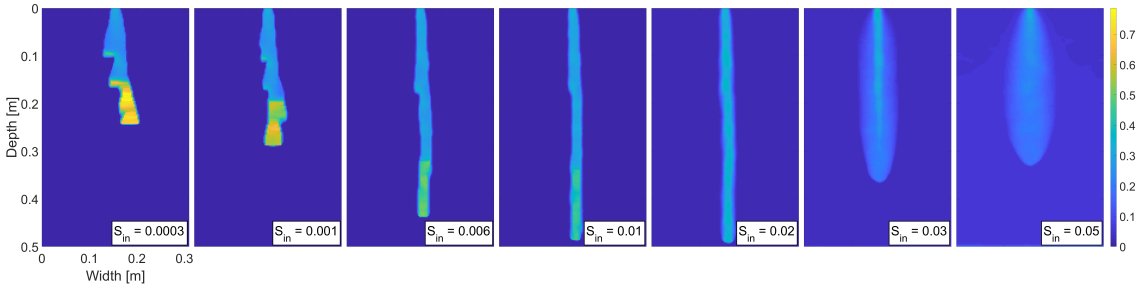

Figure A6. Snapshot of the saturation field at 25 minutes for seven different values of the initial saturation for the distribution which satisfies $\kappa_{max}/\kappa_{min} \approx 2.35$ (the distribution in Fig. A1f). Saturation values are colour-coded according to the colour bar on the right.

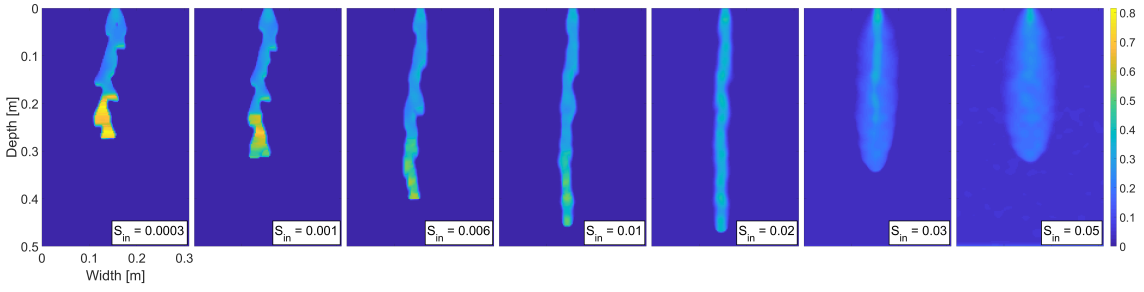

Figure A7. Snapshot of the saturation field at 25 minutes for seven different values of the initial saturation for the distribution which satisfies $\kappa_{max}/\kappa_{min} \approx 3.90$ (the distribution in Fig. A1g). Saturation values are colour-coded according to the colour bar on the right.

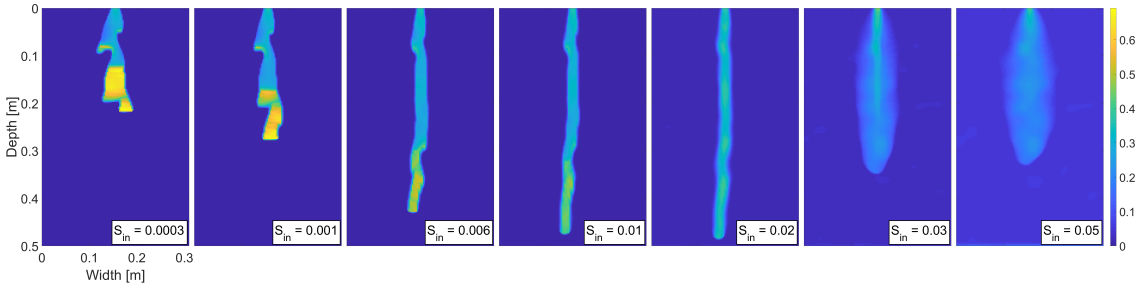

Figure A8. Snapshot of the saturation field at 25 minutes for seven different values of the initial saturation for the distribution which satisfies $\kappa_{max}/\kappa_{min} \approx 3.50$ (the distribution in Fig. A1h). Saturation values are colour-coded according to the colour bar on the right.

https://doi.org/10.5194/egusphere-2022-673
Preprint. Discussion started: 23 August 2022

Author contributions. JK and MS wrote the manuscript, TF reviewed the manuscript, TF, MS, RV and JK proposed the model, JK implemented the computer code and ran the simulations, RV checked the mathematics.

Competing interests. The authors declare that they have no conflict of interest.

Acknowledgements. Jakub Kmec, Tomáš Fürst and Rostislav Vodák gratefully acknowledge the support by the Operational Programme Research, Development and Education, project no. CZ.02.1.01/0.0/0.0/17_049/0008422 of the Ministry of Education, Youth and Sports of the Czech Republic. Rostislav Vodák was supported by the Ministry of Education, Youth and Sports of the Czech Republic, project no. CZ.02.1.01/0.0/0.0/17_049/0008408 Hydrodynamic Design of Pumps. Computational resources were supplied by the project "e-Infrastruktura CZ" (e-INFRA LM2018140) provided within the program Projects of Large Research, Development and Innovations Infrastructures. Tomáš Fürst gratefully acknowledges the generous support of the Fulbright Commission in scope of the Masaryk-Fulbright Scholarship.

https://doi.org/10.5194/egusphere-2022-673
Preprint. Discussion started: 23 August 2022

References

Al-Raoush, R.: Change in Microstructure Parameters of Porous Media Over Representative Elementary Volume for Porosity, Particulate Science and Technology, 30(1), 1–16, https://doi.org/10.1080/02726351.2010.543262, 2012.

Al-Raoush, R. and Papadopoulos, A.: Representative elementary volume analysis of porous media using X-ray computed tomography, Powder Technology, 200, 69–77, https://doi.org/10.1016/j.powtec.2010.02.011, 2010.

Aminzadeh, B. and DiCarlo, D. A.: The Transition between Sharp and Diffusive Wetting Fronts as a Function of Imbibing Fluid Properties, Vadose Zone J., 9(3), 588–596, https://doi.org/10.2136/vzj2009.0072, 2010.

Bauters, T. W. J., DiCarlo, D. A., Steenhuis, T., and Parlange, J.-Y.: Soil water content dependent wetting front characteristics in sands, J. Hydrol., 231-232, 244–254, https://doi.org/10.1016/S0022-1694(00)00198-0, 2000.

Bear, J.: Dynamics of Fluids in Porous Media, American Elsevier Publishing Company, 1972.

Beljadid, A., Cueto-Felgueroso, L., and Juanes, R.: A continuum model of unstable infiltration in porous media endowed with an entropy function, Advances in Water Resources, 144, 103 684, https://doi.org/10.1016/j.advwatres.2020.103684, 2020.

Blunt, M. J. and Scher, H.: Pore-level modelling of wetting, Phys. Rev. E, 52, 6387–6403, https://doi.org/10.1103/PhysRevE.52.6387, 1995.

Brindt, N. and Wallach, R.: The moving-boundary approach for modeling 2D gravity-driven stable and unstable flow in partially wettable soils, Water Resour. Res., 56(5), e2019WR025 772, https://doi.org/10.1029/2019WR025772, 2020.

Cahine, M.: The hydrological cycle and its influence on climate, Nature, 359, 373–380, https://doi.org/10.1038/359373a0, 1992.

Chapwanya, M. and Stockie, J.: Numerical simulations of gravity-driven fingering in unsaturated porous media using a nonequilibrium model, Water Resour. Res., 46(9), https://doi.org/10.1029/2009WR008583, 2010.

Chen, L., He, A., Zhao, J., Kang, Q., Li, Z.-Y., Carmeliet, J., Shikazono, N., and Tao, W.-Q.: Pore-scale modeling of complex transport phenomena in porous media, Progress in Energy and Combustion Science, 88, 100 968, https://doi.org/10.1016/j.pecs.2021.100968, 2022a.

Chen, L., Qiu, Q., Wang, P., Zhang, X., and Zhang, Z.: Visualization study on preferential flow in highly saturated and super hydrophilic porous media by combining dye tracking and infrared imaging, Journal of Hydrology, 612, 128 077, https://doi.org/10.1016/j.jhydrol.2022.128077, 2022b.

Cremer, C. J. M., Schuetz, C., Neuweiler, I., Lehmann, P., and Lehmann, E. H.: Unstable Infiltration Experiments in Dry Porous Media, Vadose Zone J., 16 (7), https://doi.org/10.2136/vzj2016.10.0092, 2017.

Cueto-Felgueroso, L., Suarez-Navarro, M. J., Fu, X., and Juanes, R.: Numerical Simulation of Unstable Preferential Flow during Water Infiltration into Heterogeneous Dry Soil, Water, 12(3), 909, https://doi.org/10.3390/w12030909, 2020.

DiCarlo, D. A.: Experimental measurements of saturation overshoot on infiltration, Water Resour. Res., 40(4), W04 215, https://doi.org/10.1029/2003WR002670, 2004.

DiCarlo, D. A.: Can continuum extensions to multiphase flow models describe preferential flow?, Vadose Zone J., 9(2), 268–277, https://doi.org/10.2136/vzj2009.0099, 2010.

DiCarlo, D. A.: Stability of gravity-driven multiphase flow in porous media: 40 Years of advancements, Water Resour. Res., 49, 4531–4544, https://doi.org/10.1002/wrcr.20359, 2013.

Eliassi, M. and Glass, R. J.: On the porous-continuum modeling of gravity-driven fingers in unsaturated materials: Extension of standard theory with a hold-back-pile-up effect, Water Resour. Res., 38(11), 16–1–16–11, https://doi.org/10.1029/2001WR001131, 2002.

Ewing, R. P., Hu, Q., and Liu, C.: Scale dependence of intragranular porosity, tortuosity, and diffusivity, Water Resources Research, 46, https://doi.org/10.1029/2009WR008183, 2010.

https://doi.org/10.5194/egusphere-2022-673
Preprint. Discussion started: 23 August 2022

Fürst, T., Vodák, R., Šír, M., and Bíl, M.: On the incompatibility of Richards' equation and finger-like infiltration in unsaturated homogeneous porous media, Water Resour. Res., 45(3), W03 408, https://doi.org/10.1029/2008WR007062, 2009.

Ghanbarian, B., Taslimitehrani, V., Dong, G., and Pachepsky, Y. A.: Sample dimensions effect on prediction of soil water retention curve and saturated hydraulic conductivity, Journal of Hydrology, 528, 127–137, https://doi.org/10.1016/j.jhydrol.2015.06.024, 2015.

Ghanbarian, B., Taslimitehrani, V., and Pachepsky, Y. A.: Accuracy of sample dimension-dependent pedotransfer functions in estimation of soil saturated hydraulic conductivity, CATENA, 149, 374–380, https://doi.org/10.1016/j.catena.2016.10.015, 2017.

Ghanbarian, B., Esmaeilpour, M., Ziff, R. M., and Sahimi, M.: Effect of Pore-Scale Heterogeneity on Scale-Dependent Permeability: Pore-Network Simulation and Finite-Size Scaling Analysis, Water Resources Research, 57, e2021WR030 664, https://doi.org/10.1029/2021WR030664, 2021.

Glass, R. J. and Yarrington, L.: Analysis of wetting front instability using modified invasion percolation theory, Eos Trans. AGU, 70, 1117, 1989.

Glass, R. J. and Yarrington, L.: Mechanistic modeling of fingering, nonmonotonicity, fragmentation, and pulsation within gravity/buoyant destabilized two-phase/unsaturated flow, Water Resour. Res., 39(3), 1058, https://doi.org/10.1029/2002WR001542, 2003.

Glass, R. J., Parlange, J.-Y., and Steenhuis, T. S.: Wetting front instability as a rapid and farreaching hydrologic process in the vadose zone P.F. Germann (Ed.), Rapid and farreaching hydrologic processes in the vadose zone, J. Contam. Hydrol., 3(2-4), 207–226, https://doi.org/10.1016/0169-7722(88)90032-0, 1988.

Glass, R. J., Parlange, J.-Y., and Steenhuis, T. S.: Mechanism for finger persistence in homogenous unsaturated, porous media: Theory and verification, Soil Science, 148(1), 60–70, https://doi.org/10.1097/00010694-198907000-00007, 1989a.

Glass, R. J., Parlange, J.-Y., and Steenhuis, T. S.: Wetting front instability. 2. Experimental determination of relationships between system parameters and two-dimensional unstable flow field behavior in initially dry porous media, Water Resour. Res., 25(6), 1195–1207, https://doi.org/10.1029/WR025i006p01195, 1989b.

Hassanizadeh, S. M., Celia, M. A., and Dahle, H. K.: Dynamic effects in the capillary pressure-saturation relationship and its impact on unsaturated flow, Vadose Zone J., 1, 38–57, https://doi.org/10.2136/vzj2002.3800, 2002.

Hunt, A. G., Ewing, R. P., and Horton, R.: What's wrong with soil physics, Soil Science Society of America Journal, 77, 1877– 1887, https://doi.org/10.2136/sssaj2013.01.0020, 2013.

Joekar-Niasar, V. and Hassanizadeh, S. M.: Effect of Initial Hydraulic Conditions on Capillary Rise in a Porous Medium: Pore-Network Modeling, Vadose Zone J., 11(3), https://doi.org/doi.org/10.2136/vzj2011.0128, 2012.

Kmec, J.: Analysis of the mathematical models for unsaturated porous media flow, Ph.D. thesis, Palacký University in Olomouc, Czech Republic, 2021.

Kmec, J.: The semi-continuum model for unsaturated porous media flow, Zenodo [code], https://doi.org/10.5281/zenodo.6837742, 2022.

Kmec, J., Fürst, T., Vodák, R., and Šír, M.: A semi-continuum model of saturation overshoot in one dimensional unsaturated porous media flow, Scient. Rep., 9, 8390, https://doi.org/10.1038/s41598-019-44831-x, 2019.

Kmec, J., Fürst, T., Vodák, R., and Šír, M.: A two dimensional semi-continuum model to explain wetting front instability in porous media, Scient. Rep., 11, 3223, https://doi.org/10.1038/s41598-021-82317-x, 2021.

Kmec, J., Šír, M., Fürst, T., and Vodák, R.: Simulation data for: Semi-continuum modelling of unsaturated porous media flow to explain the Bauters' paradox, Zenodo [data set], https://doi.org/10.5281/zenodo.6860668, 2022.

Kotwicki, V.: Water balance of Earth / Bilan hydrologique de la Terre, Hydrological Sciences Journal, 54, 829–840, https://doi.org/10.1623/hysj.54.5.829, 2009.

https://doi.org/10.5194/egusphere-2022-673
Preprint. Discussion started: 23 August 2022

Kouznetsova, V., Brekelmans, W. A. M., and Baaijens, F. P. T.: An approach to micro-macro modeling of heterogeneous materials, Computational Mechanics, 27, 37–48, https://doi.org/10.1007/s004660000212, 2001.

Kutílek, M. and Nielsen, D.: Soil Hydrology, Catena Verlag, Germany, 1994.

Larson, R. G. and Morrow, N. R.: Effects of sample size on capillary pressures in porous media, Powder Technology, 30(2), 123–138, https://doi.org/10.1016/0032-5910(81)80005-8, 1981.

Lenormand, R., Zacone, C., and Sarr, A.: Mechanisms of the displacement of one fluid by another in a network of capillary ducts, J. Fluid Mech., 135, 337–353, https://doi.org/10.1017/S0022112083003110, 1983.

Lenormand, R., Touboul, E., and Zarcone, C.: Numerical models and experiments on immiscible displacement in porous media, J. Fluid Mech., 189, 165–187, https://doi.org/10.1017/S0022112088000953, 1988.

Liu, H.-H.: Fluid Flow in the Subsurface – History, Generalization and Applications of Physical Laws, Springer International Publishing Switzerland, 2017.

Liu, H.-H., Zhang, R., and Bodvarsson, G. S.: An active region model for capturing fractal flow patterns in unsaturated soils: Model development, Journal of Contaminant Hydrology, 80, 18–30, https://doi.org/10.1016/j.jconhyd.2005.07.002, 2005.

Masoodi, R. and Pillai, K. M.: Wicking in Porous Materials: Traditional and Modern Modeling Approaches, Taylor & Francis, 2012.

Mishra, B. K. and Sharma, M. M.: Measurement of pore size distributions from capillary pressure curves, American Institute of Chemical Engineers Journals, 34(4), 684–687, https://doi.org/10.1002/aic.690340420, 1988.

Mualem, Y.: A new model for predicting the hydraulic conductivity of unsaturated porous media, Water Resour. Res., 12(3), 513–522, https://doi.org/10.1029/WR012i003p00513, 1976.

Mualem, Y. and Dagan, G.: Hydraulic conductivity of soils: unified approach to the statistical models, Soil Sci. Soc. Am. J., 42, 392–395, https://doi.org/10.2136/sssaj1978.03615995004200030003x, 1978.

Nimmo, J. R.: The Processes of Preferential Flow in the Unsaturated Zone, Soil Science Society of America Journal, 85, 1–27, https://doi.org/10.1002/saj2.20143, 2021.

Ommi, S. H., Sciarra, G., and Kotronis, P.: A phase field model for partially saturated geomaterials describing fluid–fluid displacements. Part I: The model and one-dimensional analysis, Advances in Water Resources, 164, 104 170, https://doi.org/10.1016/j.advwatres.2022.104170, 2022a.

Ommi, S. H., Sciarra, G., and Kotronis, P.: A phase field model for partially saturated geomaterials describing fluid–fluid displacements, Part II: Stability analysis and two-dimensional simulations, Advances in Water Resources, 164, 104 201, https://doi.org/10.1016/j.advwatres.2022.104201, 2022b.

Pales, A. R., Li, B., Clifford, H. M., Kupis, S., Edayilam, N., Montgomery, D., W.-Z. Liang, M. Dogan, N. T., Martinez, N., Moysey, S., Powell, B., and Darnault, C. J. G.: Preferential flow systems amended with biogeochemical components: imaging of a two-dimensional study, Hydrol. E. Sys. Sci., 22(4), 2487–2509, https://doi.org/10.5194/hess-22-2487-2018, 2018.

Parker, J. C. and Lenhard, R. J.: A model for hysteretic constitutive relations governing multiphase flow: 1. Saturation-pressure relations, Water Resour. Res., 23(12), 2187–2196, https://doi.org/10.1029/WR023i012p02187, 1987.

Perfect, E., McKay, L. D., Cropper, S. C., Driese, S. G., Kammerer, G., and Dane, J. H.: Capillary Pressure–Saturation Relations for Saprolite: Scaling With and Without Correction for Column Height, Vadose Zone Journal, 3(2), 493–501, https://doi.org/10.2136/vzj2004.0493, 2004.

https://doi.org/10.5194/egusphere-2022-673
Preprint. Discussion started: 23 August 2022

Primkulov, B. K., Talman, S., Khaleghi, K., Rangriz Shokri, A., Chalaturnyk, R., Zhao, B., MacMinn, C. W., and Juanes, R.: Quasistatic fluid-fluid displacement in porous media: Invasion-percolation through a wetting transition, Phys. Rev. Fluids, 3, 104 001, https://doi.org/10.1103/PhysRevFluids.3.104001, 2018.

Primkulov, B. K., Pahlavan, A. A., Fu, X., Zhao, B., MacMinn, C. W., and Juanes, R.: Signatures of fluid–fluid displacement in porous media: wettability, patterns and pressures, Journal of Fluid Mechanics, 875, R4, https://doi.org/10.1017/jfm.2019.554, 2019.

Raats, P. A. C.: Unstable wetting fronts in uniform and nonuniform soils, Soil Sci. Soc. Am. J., 37(5), 681–685, https://doi.org/10.2136/sssaj1973.03615995003700050017x, 1973.

Rätz, A. and Schweizer, B.: Hysteresis models and gravity fingering in porous media, Z. Angew. Math. Mech., 94(7-8), 645–654, https://doi.org/10.1002/zamm.201200052, 2013.

Rezanezhad, F., Vogel, H.-J., and Roth, K.: Experimental study of fingered flow through initially dry sand, Hydrol. E. Sys. Sci. D., 3(4), 2595–2620, hal-00298761, 2006.

Richards, L. A.: Capillary conduction of liquid through porous media, Physics, 1, 318–333, https://doi.org/10.1063/1.1745010, 1931.

Rooij, G. H.: Modeling fingered flow of water in soils owing to wetting front instability: a review., J. Hydrol., 231-232, 277–294, https://doi.org/10.1016/S0022-1694(00)00201-8, 2000.

Schaap, M. and Leij, F.: Improved Prediction of Unsaturated Hydraulic Conductivity with the Mualem-van Genuchten Model, Soil Science Society of America Journal, 64, 843–851, https://doi.org/10.2136/sssaj2000.643843x, 2000.

Schneider, M., Köppl, T., Helmig, R., Steinle, R., and Hilfer, R.: Stable propagation of saturation overshoots for two-phase flow in porous media, Transp. Por. Med., 121, 621–641, https://doi.org/10.1007/s11242-017-0977-y, 2017.

Schroth, M., Ahearn, S., Selker, J., and Istok, J.: Characterization of Miller-similar silica sands for laboratory hydrologic studies, Soil Science Society of America journal, 60, 1331–1339, https://doi.org/10.2136/sssaj1996.03615995006000050007x, 1996.

Schweizer, B.: Hysteresis in porous media: Modelling and analysis, Interfaces and Free Boundaries, 19 (3), 417–447, https://doi.org/10.4171/IFB/388, 2017.

Selker, J., Parlange, J.-Y., and Steenhuis, T.: Fingered flow in two dimensions: 2. Predicting finger moisture profile, Water Resour. Res., 28, 2523–2528, https://doi.org/10.1029/92WR00962, 1992.

Sililo, O. T. N. and Tellam, J. H.: Fingering in Unsaturated Zone Flow: A Qualitative Review with Laboratory Experiments on Heterogeneous Systems, Ground Water, 38(6), 864–871, https://doi.org/10.1111/j.1745-6584.2000.tb00685.x, 2005.

Silva, M. L. N., Libardi, P. L., and Gimenes, F. H. S.: Soil water retention curve as affected by sample height, Rev. Bras. Cienc. Solo, 42, e0180 058, https://doi.org/10.1590/18069657rbcs20180058, 2018.

Van Genuchten, M. T.: A closed-form equation for predicting the hydraulic conductivity of unsaturated soils, Soil Sci. Soc. Am. J., 44, 892–898, https://doi.org/10.2136/sssaj1980.03615995004400050002x, 1980.

Visintin, A.: Differential models of hysteresis, New York: Springer, 1993.

Vodák, R., Fürst, T., Šír, M., and Kmec, J.: The difference between semi-continuum model and Richards' equation for unsaturated porous media flow, Scient. Rep., 12, 7650, https://doi.org/10.1038/s41598-022-11437-9, 2022.

Wei, H., Zhu, X., Liu, X., Yang, H., Tao, W.-Q., and Chen, L.: Pore-scale study of drainage processes in porous media with various structural heterogeneity, International Communications in Heat and Mass Transfer, 132, 105 914, https://doi.org/10.1016/j.icheatmasstransfer.2022.105914, 2022.

Wei, Y., Cejas, C. M., Barrois, R., Dreyfus, R., and Durian, D. J.: Morphology of Rain Water Channeling in Systematically Varied Model Sandy Soils, Physical Review Applied, 2, 044 004, https://doi.org/10.1103/PhysRevApplied.2.044004, 2014.

https://doi.org/10.5194/egusphere-2022-673
Preprint. Discussion started: 23 August 2022

White, J. A., Borja, R. I., and Fredrich, J. T.: Calculating the effective permeability of sandstone with multiscale lattice Boltzmann/finite element simulations, Acta Geotechnica, 1, 195–209, https://doi.org/10.1007/s11440-006-0018-4, 2006.

Wilkinson, D.: Percolation effects in immiscible displacement, Phys. Rev. A, 34, 1380, https://doi.org/10.1103/PhysRevA.34.1380, 1986.

Xiong, Y.: Flow of water in porous media with saturation overshoot: A review, J. Hydrol., 510, 353–362, https://doi.org/10.1016/j.jhydrol.2013.12.043, 2014.

Yao, T. and Hendrickx, J. M. H.: Stability of wetting fronts in dry homogeneous soils under low infiltration rates, Soil Sci. Soc. Am. J., 60, 20–28, https://doi.org/10.2136/sssaj1996.03615995006000010006x, 1996.

Zhou, D. and Stenby, E. H.: Interpretation of capillary-pressure curves using invasion percolation theory, Transport Porous Med., 11, 17–31, https://doi.org/10.1007/BF00614632, 1993.